Revista Mexicana de Astronomía y Astrofísica, **54**, 363–373 (2018)

EXACT TRAVELING WAVE SOLUTIONS OF KDV EQUATION FOR DAWS IN SUPERTHERMAL PLASMA

U. M. Abdelsalam[1] and M. S. Zobaer[2]

Received January 29 2018; accepted June 5 2018

ABSTRACT

A propagation of fully nonlinear dust-acoustic waves (DAWs) in superthermal plasma is investigated. The plasma is described by the hydrodynamic dust fluid equations with superthermal electrons and ions, where both follow a kappa distribution. The reductive perturbation method is used to analyze small but finite amplitudes nonlinear DAWs. Extended homogeneous balance method is applied to obtain the exact traveling wave solutions for the Korteweg-de Vries (KdV) equation. The solutions are numerically analyzed to study the characteristics of arbitrary and small but finite amplitudes DAWs. This study is important for understanding the nonlinear excitations that may appear in astrophysical plasma objects such as the Jupiter magnetosphere.

RESUMEN

Se investiga la propagación de ondas acústicas con polvo no lineales (DAWs) en un plasma supratérmico. Se describe el plasma con las ecuaciones hidrodinámicas de un fluido con polvo, incluyendo electrones supratérmicos e iones, ambos con una distribución kappa. Se usa el método reductivo de perturbaciones para analizar DAWs no lineales con amplitudes pequeñas pero finitas. Se aplica el método de balance homogéneo extendido para obtener las soluciones exactas de las ecuaciones de Korteweg-de Vries (KdV) para la propagación de ondas. Se analizan numéricamente las soluciones para estudiar las características de los DAWs con amplitudes arbitrarias y pequeñas. Este estudio es importante para entender las excitaciones no lineales que pueden presentarse en plasmas astrofísicos, como la magnetosfera de Júpiter.

Key Words: hydrodynamics — plasmas — waves

1. INTRODUCTION

Nowadays the κ distribution is the focus in the model of space plasmas (Hasegawa et al. 1985; Sabry et al. 2012; Saini and Kourakis 2008; Saini et al. 2009; Saini and Kourakis 2010). Note that for all velocities, the κ distribution function approaches the Maxwellian distribution (which is considered a special case) for very large κ ($\kappa \to \infty$). Particles described by κ distribution are found in many kinds of plasma environments like the solar wind, the Earth's magnetospheric plasma sheet, Jupiter, and Saturn (Abdelsalam 2013; El-Shewy et al. 2011; Hellberg and Mace 2002; Leubner 2004; Sabry et al. 2012).

The inclusion of superthermal particles in a plasma characterizes the high energy region in space, and the presence of superthermal particles causes velocity space diffusion (Hasegawa et al. 1985). Many authors used the kappa distribution to study superthermal particles (ions, positrons, and electrons) (Abdelsalam et al. 2008; Ali et al. 2007; Pakzad 2011). A one-dimensional kappa distribution along a preferred direction in space and a Maxwellian distribution perpendicular to it were the focus of many studies (Hellberg and Mace 2002; Kourakis and Williams 2013). However, few works dealt with superthermal ions (as in Hellberg and Mace 2002; Saini

[1]Department of Mathematics, Faculty of Science, Fayoum University, Fayoum, Egypt.
[2]Department of Physics, Bangladesh University of Textiles, Dhaka 1208, Bangladesh.

and Kourakis 2008). Kappa distributions are more suitable to study the solar wind (Pierrard and Lemaire 1996), Jupiter and Saturn (Krimigis et al. 1983) or to explain spacecraft data in the Earth's magnetospheric plasma sheet (Christon et al. 1988) and the velocity filtration effect in the solar corona (Pierrard and Lemaire 1996).

Schippers et al. (2008) analyzed the CAPS/ELS and MIMI/ LEMMS data from the Cassini spacecraft orbiting Saturn over a range of 5.420 Rs, where $Rs \approx 60300$ km is the radius of Saturn (Alam et al. 2013). For Saturn's F-ring the nonlinear structure could be due to solitons for a very short range of plasma parameters and the largest possible solitary waves generated in plasma system with kappa-distribution with a specific velocity distribution are found to be smaller than those found in a Maxwell-Boltzmann plasma (Pakzad 2011; Saini et al. 2009; Shukla and Silin 1992). Recently, DAWs became interesting for nonlinear waves because dust particles are found in interstellar clouds (Abdelsalam 2013; El-Shewy et al. 2011; Leubner 2004; Moslem et al. 2010; Sabry et al. 2012; Shukla and Silin 1992). Depending on the nature of the charge and mass density of the dust grains, it is possible to calculate the phase velocity and the corresponding frequency for any wave as well as for a plasma system.

Here, we consider a simple model discussed in § 2 to study the effective superthermal phenomena for both electrons and ions in astrophysical compact objects and space. First, we derive the Sagdeev potential to study the large amplitude wave structure in § 3. We also derive the KdV equation with its solution for solitary nonlinear waves using a reductive perturbation method as discussed in § 4. Finally an extended homogeneous balance method is used to solve the KdV equation (Abdelsalam et al. 2008; Abdelsalam 2010; Pakzad 2011) in § 5. The numerical analysis is presented in § 6. The conclusion is summarized in § 7.

2. BASIC EQUATIONS

We considered a plasma system containing both superthermal electrons and ions with a kappa distribution, and heavy dust particles positively charged, i.e., our plasma model is composed of dust, superthermal ions and electrons. The nonlinear propagation of the electrostatic DAWs is described by

$$\frac{\partial n_d}{\partial t} + \frac{\partial}{\partial x}(n_d u_d) = 0, \tag{1}$$

$$\frac{\partial u_d}{\partial t} + u_d \frac{\partial u_d}{\partial x} + \frac{\partial \phi}{\partial x} = 0, \tag{2}$$

$$\frac{\partial^2 \phi}{\partial x^2} = n_e - n_d - n_i, \tag{3}$$

where the ions and electrons obey the κ distribution law (Pakzad 2011) as follows:

$$n_e = \left[1 - \frac{\phi}{\kappa - 3/2}\right]^{-\kappa + \frac{1}{2}}, \tag{4}$$

and

$$n_i = \mu_i \left[1 - \sigma \frac{\phi}{\kappa - 3/2}\right]^{-\kappa + \frac{1}{2}}, \tag{5}$$

where κ is a real parameter measuring the deviation of the potential energy from the Boltzmann distribution. In the limit $\kappa \to \infty$, the superthermal distribution reduces to the Boltzmann distribution.

In the last equations, n_j is the number density (where $j = i, d, e$), u_d is the dust fluid velocity, ϕ is the electrostatic potential, and $\sigma = T_e/T_i$ is the unperturbed electron-to-ion temperature ratio. At equilibrium, we have $\mu_d + \mu_i = 1$, where $\mu_d = n_{d0}/n_{e0}$, $\mu_i = n_{i0}/n_{e0}$, and n_{d0} is the unperturbed dust number density (Abdelsalam et al. 2008).

3. LARGE AMPLITUDE OF THE SAGDEEV-LIKE POTENTIAL AND NUMERICAL ANALYSIS

First, we derive a Sagdeev-type pseudo-potential as an energy balance-like equation (Abdelsalam 2010) and then we numerically solve the equation to study the properties of both the Sagdeev-like potential and a solitary pulse.

To study the finite amplitude DASWs and their properties, we assume that the dependent variables in equations (1)–(5) depend on one variable $\eta = x - Mt$, where M is the Mach number (soliton velocity/C_{sd}) and η has been normalized by λ_D. Thus, we obtain from equations (1) and (2) that $n_d = \mu_d \left(\sqrt{1 - \frac{2\phi}{M^2}}\right)^{-1}$. Then, by substituting n_d, n_e and n_i into Poisson equation [equation (3)], and multiplying the left and right sides of the obtained equation by $d\phi/d\eta$, we can integrate the equation and apply the boundary conditions, $\phi \to 0$ and $d\phi/d\eta \to 0$ at $\eta \to \pm\infty$; we get

$$\frac{1}{2}\left(\frac{d\phi}{d\eta}\right)^2 + V(\phi) = 0, \tag{6}$$

where the Sagdeev potential for our purposes reads

$$V(\phi) = \left(1 - \left[1 - \frac{\phi}{\kappa - 3/2}\right]^{-\kappa+\frac{3}{2}}\right) - \frac{\mu_i}{\sigma}\left(1 - \left[1 - \sigma\frac{\phi}{\kappa - 3/2}\right]^{-\kappa+\frac{3}{2}}\right) + \mu_d M^2\left[1 - \left(1 - \frac{2\phi}{M^2}\right)^{1/2}\right]. \tag{7}$$

Equation (7) can be regarded as an 'energy integral' of an oscillating particle of unit mass, with a velocity $d\phi/d\eta$ and position ϕ in a potential $V(\phi)$.

If the DASWs exist, then the Sagdeev potential needs to satisfy the following conditions: (a) at $\phi = 0$, $d^2V/d\phi^2 < 0$; (b) we can find a critical value (max. or min. value of ϕ) ϕ_m, at which $V(\phi_m) = 0$; and (c), when $V(\phi) < 0$ then we find $0 < \phi < \phi_m$. So we can obtain the maximum and minimum values of the Mach number M for which solitons exist. Using the condition (a), the lower limit of Mach number M is $\sqrt{(\frac{2\kappa-3}{2\kappa-1})(\frac{\mu_d}{1-\sigma\mu_i})}$. The maximum number of M can be obtained by the condition $V(\phi_c) \geq 0$, where $\phi_c = M^2/2$ is the minimum value of ϕ for which the ion density is real. Thus, we have

$$\left(\left[1 - \frac{M^2}{2\kappa - 3}\right]^{-\kappa+\frac{3}{2}} - 1\right) - \frac{\mu_i}{\sigma}\left(\left[1 - \sigma\frac{M^2}{2\kappa - 3}\right]^{-\kappa+\frac{3}{2}} - 1\right) > 0.$$

The latter inequality provides the maximum M, which turns out to depend on the parameters μ_i and σ. Therefore, the following inequality can help us to calculate the Mach number range

$$\sqrt{\left(\frac{2\kappa - 3}{2\kappa - 1}\right)\left(\frac{\mu_d}{1 - \sigma\mu_i}\right)} < M < \left(\left[1 - \frac{M^2}{2\kappa - 3}\right]^{-\kappa+\frac{3}{2}} - 1\right) - \frac{\mu_i}{\sigma}\left(\left[1 - \sigma\frac{M^2}{2\kappa - 3}\right]^{-\kappa+\frac{3}{2}} - 1\right). \tag{8}$$

We obtain the range of Mach number as $0.45 < M < 1.2$ for the values of $\mu_i = 0.25$ and $\sigma = 0.9$. The existence of supersonic and subsonic solitons is noted. By increasing the ratio μ_i, to $\mu_i = 0.4$, the Mach number range reads $0.45 < M < 0.99$, which shows that the increase of μ_i leads to an expansion of subsonic solitons.

In Figures 1 and 2, the Sagdeev potential in equation (8) has been numerically analyzed. Note that the profile of the potential depends on α and M. Figure 1 shows the effect of the ion-to-electron number density ratio μ_i on the compressive solitary pulse for subsonic and supersonic waves. An increase of μ_i (which means a decrease of μ_d) makes the potential deeper and wider. However, a supersonic soliton has deeper amplitude and wider depth than a subsonic soliton.

Figure 2 shows that increasing the Mach number (M) leads to the expansion of the permitted region of the potential values associated with the localized excitations, which implies that faster pulse excitations will be large and narrow. The energy in equation (6) has been numerically solved for many parameters. The profiles of the potential pulse are drawn in Figure 3. It is found that shorter pulses are wider than longer pulses and that increasing M causes an increase in the amplitude and a decrease in the width.

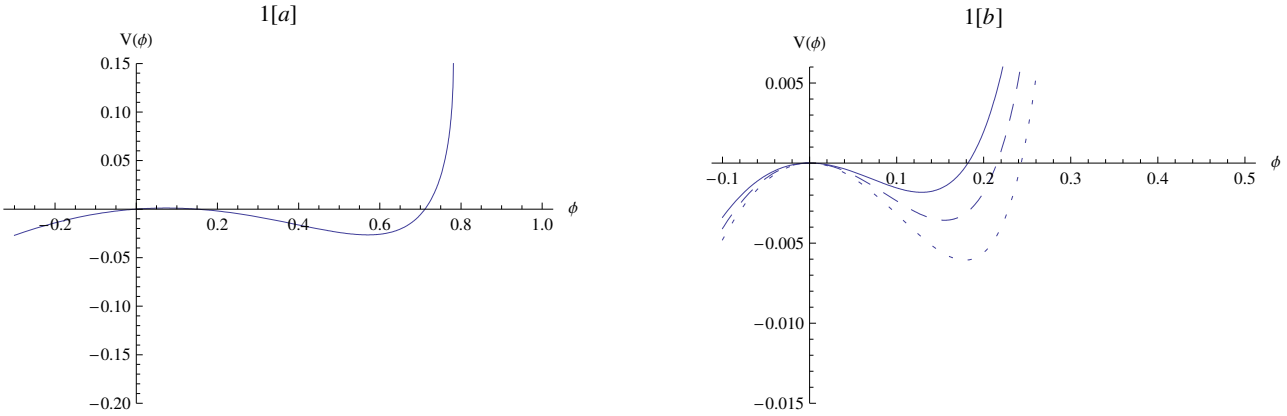

Fig. 1. The Sagdeev potential $V(\phi)$ [represented by equation (7)] against the potential ϕ. (a) supersonic solitary pulse for $M = 1.1$. (b) subsonic solitary pulse for $M = 0.8$. The effect of varying $\mu_i = 0.2$ (solid curve), $\mu_i = 0.3$ (dashed curve), and $\mu_i = 0.4$ (dotted curve), where $\sigma = 0.9$ is shown. The color figure can be viewed online.

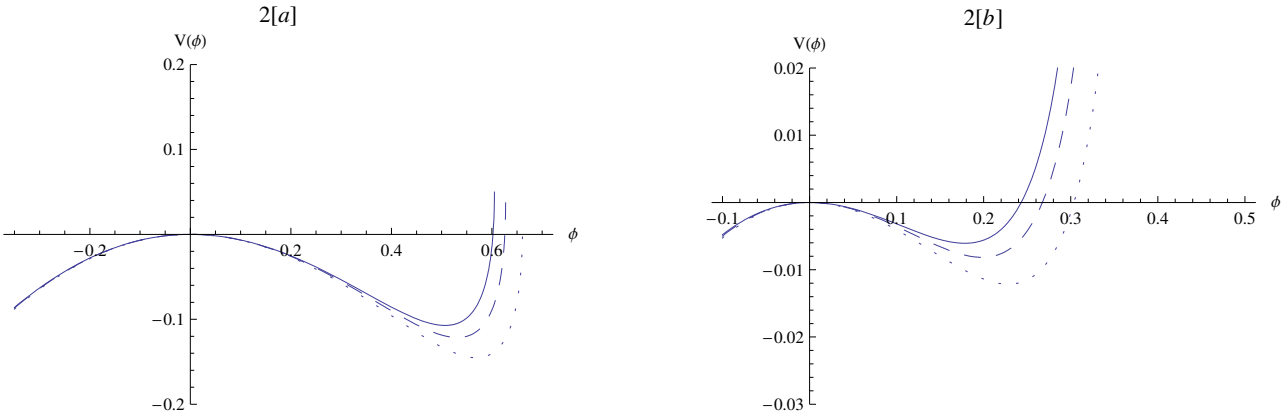

Fig. 2. The Sagdeev potential $V(\phi)$ [represented by equation (7)] against the potential ϕ. (a) supersonic solitary pulse for $M = 1.1$ (solid curve), $M = 1.15$ (dashed curve), and $M = 1.2$ (dotted curve). (b) subsonic solitary pulse for $M = 0.8$ (solid curve), $M = 0.85$ (dashed curve), and $M = 0.9$ (dotted curve). Here, $\mu_i = 0.3$ and $\sigma = 0.95$. The color figure can be viewed online.

4. KORTEWEG-DE VRIES EQUATION AND SOLUTION FOR NUMERICAL ANALYSIS

In this section, we study solitary waves with small and finite amplitude deriving the Korteweg-de Vries (KdV) equation using a nonlinear perturbation method to study dust-acoustic-solitary-waves (DASWs) (Abdelsalam 2010).

For the reductive perturbation method, we should use the stretched space-time coordinates $\xi = \varepsilon^{1/2}(x - \vartheta t)$ and $\tau = \varepsilon^{3/2}t$ (Washimi and Tanituri 1966), where ϑ is the phase speed and ε is the smallness parameter measuring the weakness of the dispersion ($0<\varepsilon<1$). The dependent variables are expanded as

$$\Psi = \Psi^{(0)} + \sum_{n=1}^{\infty} \epsilon^n \Psi^{(n)}, \tag{9}$$

where n = 0, 1, 2, 3, . . .,

$$\Psi = \{n_e, n_d, n_i, u_d, \phi\}^T, \tag{10}$$

and

$$\Psi^{(0)} = \{1, \mu_d, \mu_i, 0, 0\}^T. \tag{11}$$

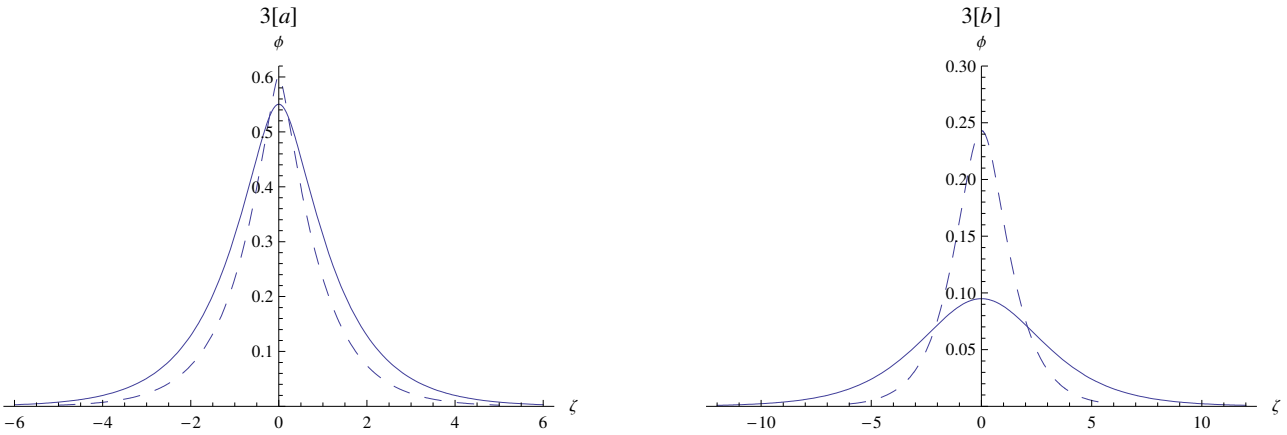

Fig. 3. The potential ϕ [the solution of equation (6)] is depicted against ζ. (a) supersonic solitary pulse for $M = 1.1$ (solid curve) and $M = 1.25$ (dashed curve). (b) subsonic solitary pulse for $M = 0.8$ (solid curve) and $M = 0.9$ (dashed curve). Here $\mu_i = 0.2$ and $\sigma = 0.8$. The color figure can be viewed online.

Using the last stretching and expansions into equations (1)–(5), we isolate distinct orders in ϵ and derive the corresponding variable contributions. The lowest-order equations in ϵ read

$$n_e^{(1)} = \left(\frac{2\kappa - 3}{2\kappa - 1}\right)\phi^{(1)}, \quad n_i^{(1)} = \mu_i\sigma\left(\frac{2\kappa - 3}{2\kappa - 1}\right)\phi^{(1)}, \quad n_d^{(1)} = \left(\mu_d/\vartheta^2\right)\phi^{(1)}, \quad u_d^{(1)} = (1/\vartheta)\phi^{(1)},$$

and

$$\vartheta = \sqrt{\left(\frac{2\kappa - 3}{2\kappa - 1}\right)\left(\frac{\mu_d}{1 - \sigma\mu_i}\right)}.$$

Note that the minimum Mach number is identically ϑ.

The next order in ϵ yields the values for $n_e^{(2)}$, $n_i^{(2)}$, $u_d^{(2)}$, and $n_d^{(2)}$. However, by solving the last equations system, we obtain the KdV equation (Malfliet 1992)

$$\frac{\partial\phi^{(1)}}{\partial\tau} + A\phi^{(1)}\frac{\partial\phi^{(1)}}{\partial\xi} + B\frac{\partial^3\phi^{(1)}}{\partial\xi^3} = 0, \tag{12}$$

where A is the nonlinear coefficient and B is the dispersion coefficient, respectively,

$$A = \frac{3}{2\vartheta} + \mu_i\vartheta^3\sigma^2\frac{4\kappa^2 - 1}{2\mu_d(2\kappa - 3)^2} - \vartheta^3\frac{4\kappa^2 - 1}{2\mu_d(2\kappa - 3)^2}, \qquad B = \frac{\vartheta^3}{2\mu_d}. \tag{13}$$

5. EXTENDED HOMOGENEOUS BALANCE METHOD TO SOLVE THE KDV EQUATION

The extended homogeneous balance (HB) method is applied to obtain many solutions for the KdV equation (Abdelsalam 2017; Abdel-Rady et al. 2010; El-Wakil et al. 2007; Wang 1995; Wang et al. 1995). Consider the KdV equation [equation (12)] as:

$$u_\tau + \alpha u u_\xi + \beta u_{\xi\xi\xi} = 0 \tag{14}$$

where α stands for A and β for B.

Applying the transformation $u(\xi, \tau) = U(\eta), \eta = \xi - \lambda\tau$ to equation (14), we find that U satisfies the following ordinary differential equation

$$-\lambda U' + \alpha U U' + \beta U''' = 0. \tag{15}$$

Integrating (15) with respect to η once, we get

$$-\lambda U + \frac{\alpha}{2}U^2 + \beta U'' = 0. \tag{16}$$

Now, balancing U^2 with U'' gives the magnitude, $|m| = 2$. Hence, the solution should be of the form

$$U = a_0 + b_0 + a_1\omega + b_1(1+\omega)^{-1} + a_2\omega^2 + b_2(1+\omega)^{-2}, \tag{17}$$

where the Riccati equation is, $\omega^{'} = k + M\ \omega + P\ \omega^2$; here, ω is the angular frequency, $\omega^{'} = d\omega/d/\xi$, k is the wave number, and M and P are the coefficient parameters; k and P cannot be zero (0).

Substituting the last equation equation (17) in equation (16), we get a polynomial equation ω. Now, equating the coefficient of ω^i $(i = 0, 1, 2, ...)$ to zero, we get a system of algebraic equations and by solving this system using package MATHEMATICA (Abdelsalam 2017), we obtain:

the first set:

$$\alpha \neq 0; \quad a_1 = -\frac{12MP\beta}{\alpha}; \quad a_2 = -\frac{12P^2\beta}{\alpha}; \quad b_1 = 0; \quad b_2 = 0; k = \frac{-2\beta M^2 - \alpha a_0}{4P\beta}; \quad \lambda = \beta M^2 + 8kP\beta + \alpha a_0; \tag{18}$$

the second set:

$$\alpha \neq 0; \quad a_0 = \frac{4\left(2kP\beta - 5P^2\beta\right)}{\alpha}; \quad a_1 = -\frac{24P^2\beta}{\alpha}; \quad a_2 = -\frac{12P^2\beta}{\alpha}; \quad b_1 = 0; \quad b_2 = -\frac{12(\beta k^2 - 2P\beta k + P^2\beta)}{\alpha}; \\ M = 2P; \quad \lambda = 4\beta P^2 + 8k\beta P + \alpha a_0; \tag{19}$$

Four cases regarding the Riccati equation were previously published by Abdelsalam (2017). As full details of these four cases are already published, here they are not discussed. Case I is considered when $P = 1$ and $M = 0$. The Riccati equation gives two solutions for $k < 0$ and $k > 0$ separately. Case II is considered for balancing between ω' and ω^2. An arbitrary constant, $r = 1$, is used for Case III. Finally, balancing ω' with ω^2 leads to $|m| = 1$, and Case IV is introduced. We will use the case numbers in this work to explain our current study. At this stage, we encourage the readers to consult Abdelsalam (2017).

For the first set of equations (18), if $M = 0$, $P = 1$ the obtained solutions will satisfy Case I of the solutions for the Riccati equation (Abdelsalam 2017). For $k > 0$, the solutions of the KdV equation of the type of equation (14), will be

$$u_1(\xi, t) = a_0 - \frac{12k\beta \tan^2\left(\sqrt{k}\eta\right)}{\alpha}, \tag{20}$$

$$u_2(\xi, t) = a_0 - \frac{12k\beta \cot^2\left(\sqrt{k}\eta\right)}{\alpha}. \tag{21}$$

For $k < 0$,

$$u_3(\xi, t) = a_0 + \frac{12k\beta \tanh^2\left(\sqrt{-k}\eta\right)}{\alpha}, \tag{22}$$

$$u_4(\xi, t) = a_0 - \frac{12k\beta \coth^2\left(\sqrt{k}\eta\right)}{\alpha}, \tag{23}$$

For $k = 0$,

$$u_5(\xi, t) = a_0 - \frac{12\beta}{\alpha\eta^2}, \tag{24}$$

Now with the compatibility condition, we obtain the solutions satisfying Cases II, III, and IV,

$$Pk = \frac{M^2 - p_1^2}{4}. \tag{25}$$

Therefore, substituting for P and k, from (18) into (25), and solving for p_1, we find that

$$p_1 = \sqrt{\frac{3\beta M^2 + \alpha a_0}{\beta}}. \tag{26}$$

Hence, for Case II, we get the following solutions:

$$u_6(\xi,t) = a_0 - \frac{3\beta p_1^2 \left(M + 2\tanh\left(\eta p_1\right)\right)^2}{\alpha} + \frac{6M\beta p_1 \left(M + 2\tanh\left(\eta p_1\right)\right)}{\alpha}, \tag{27}$$

and

$$u_7(\xi,t) = a_0 - \frac{3\beta \left(M + 2\coth\left(\eta p_1\right)\right)^2 p_1^2}{\alpha} + \frac{6M\beta \left(M + 2\coth\left(\eta p_1\right)\right) p_1}{\alpha}, \tag{28}$$

For Case III, the solution is

$$u_8(\xi,t) = a_0 + \frac{3\beta}{\alpha(r+\cosh(\eta))^2}\left[\cosh(\eta)(2r+\cosh(\eta))M^2 + (M^2-1)r^2 - \sinh(\eta)(\sinh(\eta) + 2\sqrt{r^2-1}) + 1\right], \tag{29}$$

with the condition that $p_1 = 1$. Finally, for Case IV,

$$u_9(\xi,t) = a_0 - \frac{3\beta \left(M + \coth(\eta) + \operatorname{csch}(\eta)\right)^2}{\alpha} - \frac{6M\beta(M + \coth(\eta) + \operatorname{csch}(\eta))}{\alpha}, \tag{30}$$

with the condition that $p_1 = 1$, and

$$u_{10}(\xi,t) = \frac{3\beta\left(M^2 - 4\coth^2(\eta)\right) + \alpha a_0}{\alpha}, \tag{31}$$

with the condition that $p_1 = 2$.

For the second set we are left only with solutions satisfying Cases II, III, and IV. Since the main criteria for these cases to be applicable is the compatibility condition,

$$Pk = \frac{M^2 - p_1^2}{4}, \tag{32}$$

from (19), it is found that

$$p_1 = \sqrt{\frac{-3\beta M^2 - \alpha a_0}{2\beta}}. \tag{33}$$

Therefore, solutions to equations of the type of equation (14) will be

$$u_{11}(\xi,t) = \frac{4\beta}{\alpha}\left(-\frac{3(k-P)^2P^2}{(P - p_1(P + \tanh(\eta p_1)))^2} + (2k-5P)P + 6p_1(P+\tanh(\eta p_1))P - 3p_1^2(P+\tanh(\eta p_1))^2\right), \tag{34}$$

and

$$u_{12}(\xi,t) = \frac{4\beta}{\alpha}\left(-\frac{3(k-P)^2P^2}{(P - (P + \coth\eta p_1))p_1)^2} + (2k-5P)P + 6(P+\coth(\eta p_1))p_1P - 3(P+\coth(\eta p_1))^2p_1^2\right), \tag{35}$$

For Case III,

$$\begin{aligned} u_{13}(\xi,t) =& \frac{\beta}{\alpha}\left(-\frac{48(k-P)^2P^2(r+\cosh(\eta))^2}{(\sinh(\eta)+\sqrt{r^2-1})^2} - 3\left(2P + \frac{\sinh(\eta)+\sqrt{r^2-1}}{r+\cosh(\eta)}\right)^2\right. \\ &\left. +4(2k-5P)P + 12P\left(2P + \frac{\sinh(\eta)+\sqrt{r^2-1}}{r+\cosh(\eta)}\right)\right), \end{aligned} \tag{36}$$

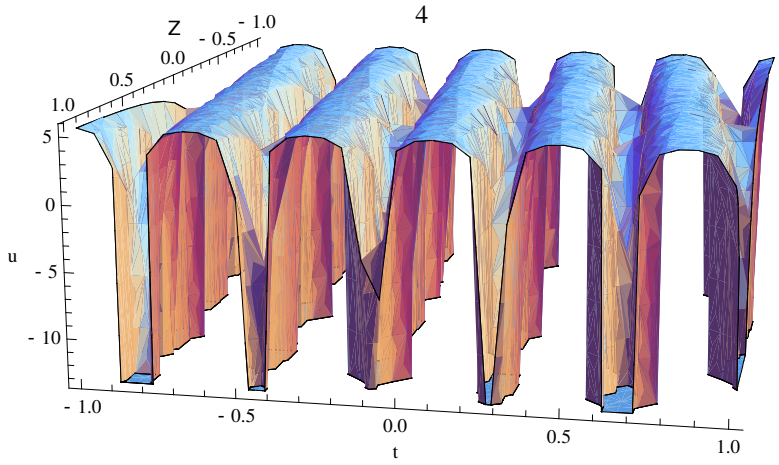

Fig. 4. 3D plots of the solution of equation (20) with $A = 0.5$ and $B = 2.9$. The color figure can be viewed online.

where $p_1 = 1$.

Finally for case IV,

$$u_{14}(\xi,t) = \frac{\beta}{\alpha}\Big(-\frac{48(k-P)^2P^2}{(4P+\coth(\eta)+\operatorname{csch}(\eta))^2} + 4(2k-5P)P - 12(2P+\coth(\eta)+\operatorname{csch}(\eta))P - 3(2P+\coth(\eta)+\operatorname{csch}(\eta))^2\Big), \tag{37}$$

with $p_1 = 1$ and

$$u_{15}(\xi,t) = -\frac{4\beta}{\alpha}\Big(3\coth^4(\eta) - 2(k-P)P\coth^2(\eta) + 3(k-P)^2P^2\Big)\tanh^2(\eta), \tag{38}$$

with the condition that $p_1 = 2$.

To investigate the nonlinear properties of solitary waves [as represented by equation (22)], for $k = -\vartheta/4\beta$ we express the solution equation (14) in the following form

$$\phi^{(1)} = \phi_0 \operatorname{sech}^2\left(\frac{\xi}{\Delta}\right), \tag{39}$$

where the amplitude is $\phi_0 = 3u_0/A$ and the width is $\Delta = (4B/u_0)^{1/2}$ for the solitary wave profiles caused by the balance between nonlinearity and dispersion. As the standard result for KdV we see that $\phi_0\Delta^2 = 12B/A =$ constant (for given ϑ) (Killian 2006).

6. NUMERICAL ANALYSIS

The extended HB is applied to give the traveling wave solutions for the KdV equation (Abdelsalam 2017; El-Wakil et al. 2007; Wang 1995). The obtained solutions cover many types of periodical, rational, singular and solitary wave solutions. As an example, the solution of equation (20) is a sinusoidal-type periodical solution shown in Figure 4. The solutions for equation (24) are of rational-type and the solution of equation (22) is a kink-type solitary wave solution. Note here that equations (23) and (31) are explosive/blowup solutions as depicted in Figure 5. The solution of equation (6) represents a soliton wave with amplitude ϕ_0.

Note that increasing the electron-to-ion temperature ratio $\sigma = T_e/T_i$ as well as the parameter κ will decrease the amplitude (as in Figure 6), while we can see in Figure 7 the effect of increasing the ion-to-electron number density ratio μ_i (which means a decrease of μ_d) which will make the soliton taller and wider. We can now

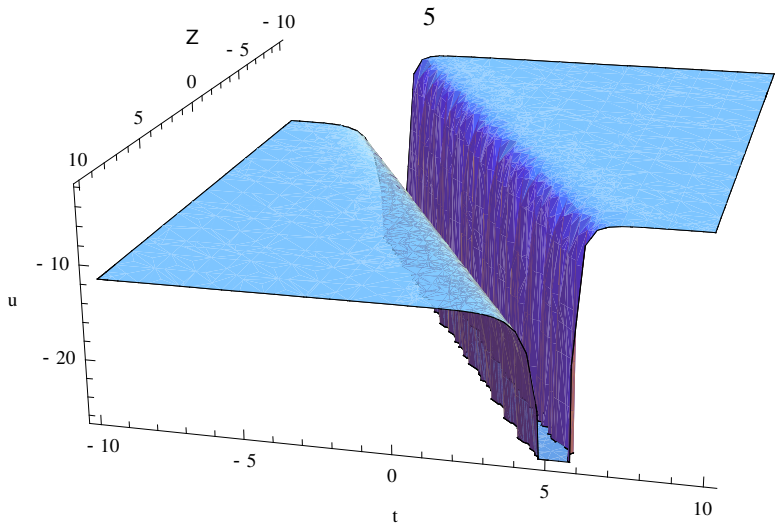

Fig. 5. 3D plots of the solution equation (30) with $A = 0.5$, $B = 2.9$ and $M = 0.9$. The color figure can be viewed online.

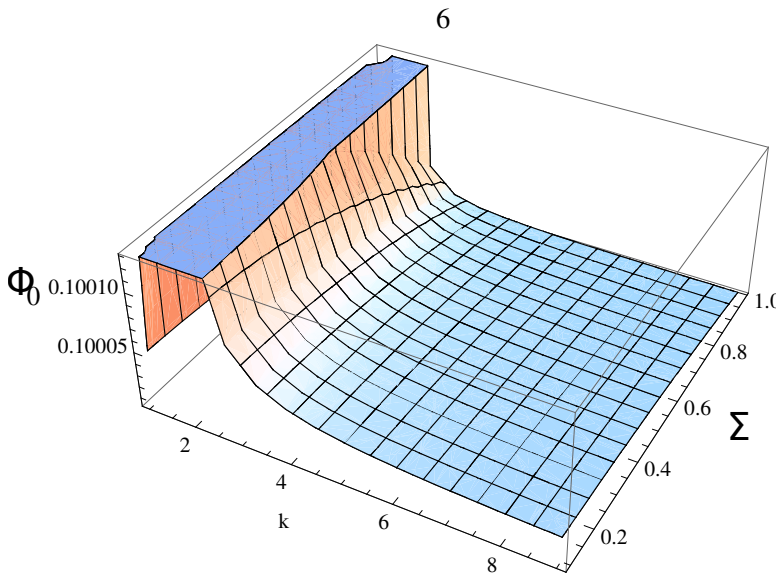

Fig. 6. The variation of the solitary pulse amplitude ϕ_0 [equation (39)] against κ and σ for fixed values of $\mu_i = 0.22$, and $\vartheta = 0.1$. The color figure can be viewed online.

compare this analytical solution to the numerical solution (obtained by numerical integration) of equation (6), in Figure 8. Note that the difference between the approximate and exact solutions increases with increasing nonlinearity, thus enhancing the amplitudes of pulses.

Overall, in this paper the nonlinear dust-acoustic solitary wave propagation is studied in a superthermal ion-electron-dust plasma. The dust is described by the hydrodynamic equations with superthermal electrons and ions. The Sagdeev equation is derived. It is shown that for low values of μ_i we can observe both supersonic and subsonic DAWs. While increasing μ_i leads to an expansion of subsonic solitons only, we discussed the reliance of the potential pulse excitation characteristics and of the pseudo-potential profiles on μ_i and the Mach number. The effects of the physical parameters have been studied on the localized DAWs structures/excitations and the propagating nonlinear structures. The extended homogeneous balance method extracts a wide range of solution structures using the techniques for solving partial differential equation (PDEs); the method is applied

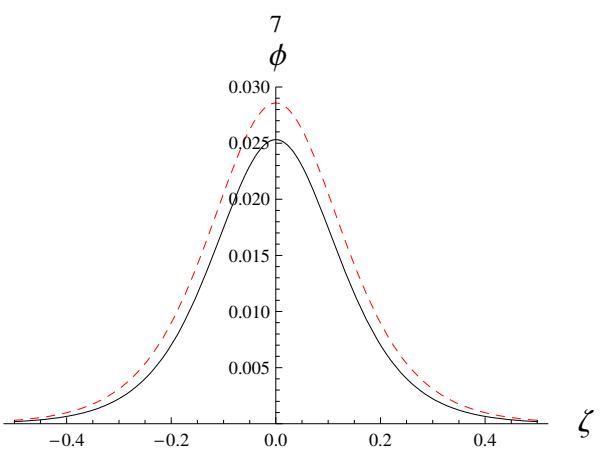

Fig. 7. The solitary potential excitation [as given by equation (39)] for varying the value of phase speed $\mu_i = 0.21$ (solid curve) and $\mu_i = 0.3$ (dashed curve) with $\kappa = 3$, $\sigma = 0.9$, and $\vartheta = 0.1$. The color figure can be viewed online.

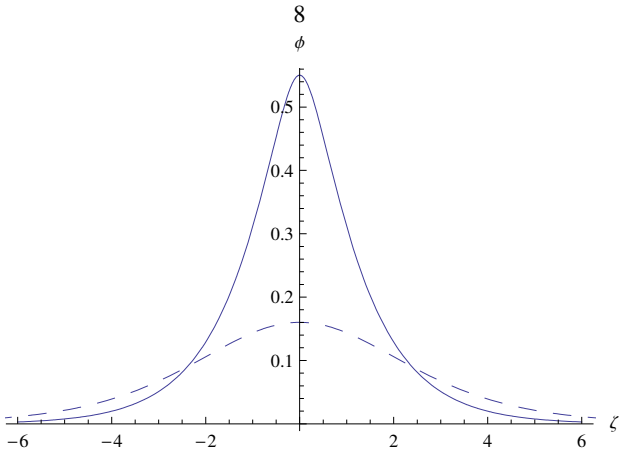

Fig. 8. The potential ϕ [exact/numerical integration of equation (7)] and the approximate potential [represented by equation (39)] are depicted against ζ. The solid and dashed curves represent the exact and approximate solutions, respectively. Here $\mu_i = 0.2$, $\sigma = 0.9$, $\kappa = 3$, $M = 1.1$, and $\vartheta = 0.1$. The color figure can be viewed online.

to the KdV equation. Many traveling wave solutions are formally derived for these equations, some of them new and interesting (Abdelsalam et al. 2008; Abdelsalam 2010, 2017; El-Wakil et al. 2007; Pakzad 2011; Wang et al. 1995). These solutions include many types of wave solutions.

7. CONCLUSION

In the previous investigations, it was confirmed that theoretically dust particles with positive charges are present in the outer magnetosphere of Jupiter and Saturn (Horanyi et al. 2004; Scarf 1969); the same speed for ions and electrons was considered to study the solitons and shock waves (Saleem et al. 2012). However, the existence of rogue waves was also found when the solar wind interacts with Jupiter's magnetosphere (Tolba et al. 2015, 2017; Abdelghany et al. 2016) in the presence of positively charged dust particles (Horanyi et al. 2004; Saleem et al. 2012). Thus, nonlinear waves are also present in Jupiter's magnetosphere and due to the presence of ions and electrons, the streaming dust acoustic wave speed effect does not contribute to the dust dynamics (Horanyi et al. 2004; Scarf 1969; Saleem et al. 2012; Tolba et al. 2015, 2017; Abdelghany et al. 2016). Thus in this work, we consider positively charged dust particles in our superthermal plasma model and study both large and small amplitude nonlinear wave propagation using the reductive perturbation method.

This work is mainly relevant to nonlinear DASWs in superthermal electrons and ions following κ distribution in an unmagnetized collisionless plasma. The dissipation of solitary waves (solution of the KdV equation) in the presence of positively charged dust particles is also studied numerically with the extended homogeneous balance method used to solve the KdV equation. Because of the large range of $\sigma(= T_e/T_i)$, the Landau damping effect on dissipation is negligible, but the damping of solitary waves is mainly caused by the ion-dust collision and the kinematic viscosity (Nakamura and Sarma 2001). Thus if we consider a viscosity term in the model the nonlinear structure for shock waves can be studied(Lu et al. 2006; Nakamura et al. 1999; Pakzad 2011). Some studies considered positrons in the plasma model as super-dense electron-positron-ion plasmas which also can be found in some astrophysical environments (Abdelsalam et al. 2008; Ali et al. 2007; Pakzad 2011).

The authors would like to express their deepest gratitude to the reviewer for his constructive comments, which significantly contributed to improve the manuscript. MSZ wants to thank Bangladesh University of Textiles, Dhaka, Bangladesh for this collaboration work.

REFERENCES

Abdelghany, A. M., Abd El-Razek, H. N., Moslem, W. M., & El-Labany, S. K. 2016, PhPl, 23, 2121

Abdel-Rady, A. S., Osman, E. S., & Khalfallah, M. 2010, CNSNS, 15, 264

Abdelsalam, U. M., Moslem, W. M., & Shukla, P. K. 2008, PhLA, 372, 4057

Abdelsalam, U. M. 2010, PhyB, 18, 3914

Abdelsalam, U. M. 2013, JPlPh, 79, 287

Abdelsalam, U. M. 2017, Journal of Ocean Engineering and Science, 2, 28

Alam, M. S., Masudb, M. M., & Mamun, A. A. 2013 ChPhB, 22, 5202

Ali, S., Moslem, W. M., Shukla, P. K., & Schlickeiser, R. 2007, PhPl, 14, 2307

Christon, S. P., et al. 1988, JGR, 93, 2562

El-Wakil, S. A., Abulwafa, E. M., Elhanbaly, A., & Abdou, M. A. 2007, CSF, 33, 1512

El-Shewy, E. K., El-Maaty, M. I. A., Abdelwahed, H. G., & Elmessary, M. A. 2011, Ap&SS, 322, 179

Hasegawa, A., Mima, K., & Duong-van, M. 1985, PhRvL, 54, 2608

Hellberg, M. A. & Mace, R. L. 2002, PhPl, 9, 1495

Horanyi, M., et al. 2004, RvGeo, 42, 4002

Killian, T. C. 2006, Natur 441, 298

Kourakis, I. & Williams, G. 2013, Modelling of multidimensional electrostatic excitations in electron-positron-ion plasmas in the presence of kappa-distributed superthermal particles; AGU Fall Meeting Abstracts, American Geophysical Union, USA

Krimigis, S. M., et al. 1983, JGR, 88, 8871

Leubner, M. P. 2004, PhPl, 11, 1308

Lu, D., Hong, B., & Tian, L. 2006, International Journal of Nonlinear Science, 2, 3

Malfliet, W. 1992, AmJPh, 60, 650

Moslem, W. M., Abdelsalam, U. M., Sabry, R., & Shukla, P. K. 2010, NJPh, 12, 3010

Nakamura, Y., Bailung, H., & Shukla, P. K. 1999, PhRvL, 83, 1602

Nakamura, Y. & Sarma, A. 2001, PhPl, 8, 3921

Pakzad, H. R. 2011, Ap&SS, 331, 169

Pierrard, V. & Lemaire, J. 1996, JGR, 101, 7923

Sabry, R., Moslem, W. M., & Shukla, P. K. 2012, PPCF, 54, 035010

Saini, N. S. & Kourakis, I. 2008, PhPl, 15, 3701

Saini, S. A., Kourakis, I., & Hellberg, M. A. 2009, PhPl, 16, 2903

Saini, N. S. & Kourakis, I. 2010, PPCF, 52, 7

Saleem, H., Moslem, W. M., & Shukla, P. K. 2012, JGRA, 117, A8

Scarf, F. L. 1969, P&SS, 17, 595

Schippers, P. et al. 2008, JGRA, 113, 7208

Shukla, P. K. & Silin, V. P. 1992, PhyS, 45, 508

Tolba, R. E., Moslem, W. M., El-Bedwehy, N. A.& El-Labany, S. K. 2015, PhPl, 22, 043707

Tolba, R. E., et al. 2017, ITPS, 45, 2552

Wang, M. L. 1995, PhLA, 199, 169

Wang, M. L., Zhou, Y. & Li, Z. 1996, PhLA, 216, 67

Washimi, H. & Taniuti, T. 1996, PhRvL, 17, 996

U. M. Abdelsalam: Department of Mathematics, Faculty of Science, Fayoum University, Fayoum, Egypt (usama.ahmad@rub.de).

William M. S. Zobaer: Department of Physics, Bangladesh University of Textiles, Dhaka 1208, Bangladesh (m.s.zobaer@butex.edu.bd).